Supplemental Materials

Supplemental Methods

Human Ventricular Tissue Samples

Human ventricular myocardium was obtained from end-stage ischemic cardiomyopathic hearts explanted at the time of cardiac transplantation. Non-failing donor hearts that were unsuitable for transplantation were used as control. Prior to explant, hearts underwent intra-operative antegrade coronary perfusion with 4:1 blood cardioplegia solution. Following arrest, hearts were explanted and placed into cold Ca^{2+}-free, modified Krebs-Henseleit solution, as previously described (63). Samples were taken from mid-myocardial regions of the LV free wall and the RV free wall, in areas void of scar tissue. Tissue samples were rapidly frozen in liquid nitrogen and stored at -80°C until RNA isolation. Patient consent, sample collection and preparation, and clinical data collection were performed according to a human subject research protocol approved by the IRB of the Lewis Katz School of Medicine at Temple University (PI: Tsai).

WGCNA

Pearson correlations were determined for each pair of expressed (average FPKM>1) and varying (coefficient of variation>10%) transcripts. Correlations were transformed to approximate a scale-free degree distribution by raising each correlation to the power of 6 as recommended by pickSoftThreshold algorithm within WGCNA. Topological Overlap (TOM) was calculated as follows:

$$TOM_{ij} = \frac{\sum_u \{A_{iu} A_{uj}\} + A_{ij}}{min(k_i, k_j) + 1 - A_{ij}}$$

where *i*, *j* are a pair of transcripts, *u* is the set of all other transcripts, *A* is the adjusted correlation matrix, and *k* is the degree of the node. Modules were identified using the dynamic tree cut algorithm on the DistTOM (1-TOM) matrix and eigengenes were determined from the first principle component of the genes in each module. Modules whose eigengenes have a Pearson correlation of greater than 0.8 were merged.

Hubs

For a given node *n* in module G, the normalized betweenness centrality $C_b(n)$ is:

$$C_b(n) = \frac{2\sum_{s\neq n\neq t}(\sigma_{st}(n)/\sigma_{st})}{(N-1)(N-2)}$$

where *s* and *t* are nodes in G different from *n*, $\sigma_{st}$is the number of shortest paths from *s* to *t* and $\sigma_{st}(n)$ represents the number of shortest paths from *s* to *t* which pass through *n*. N is the total number of nodes.

Animal experiments

Adult male C57BL/6J WT mice (Jackson Laboratory) were subjected to PAB, TAC, or Sham surgery at age 10-12 wk. Pre-operative analgesia with meloxicam SR 4mg/kg s.c. was given one day prior to surgery. Animals were anesthetized to surgical plane with ketamine/xylazine (80-100/5-10 mg/kg, i.p.), endotracheally intubated, and mechanically ventilated (MiniVent 845 Mouse Ventilator, Harvard Apparatus).

PAB model

Pulmonary artery banding was used to induce RV pressure overload and eventual RV failure in mice, as previously described (72) with slight modifications. After left thoracotomy, the pulmonary artery was carefully dissected free from the aorta and a 7-0 silk suture was gently tied around the proximal main PA, against a blunt 25g needle to yield a narrowing 0.5mm in diameter when the needle was removed.

TAC model

Transverse aortic constriction was used to induced LV pressure overload and eventual LV failure in mice, as previously described (71). Following thoracotomy, a 7-0 silk suture was tied around the transverse aorta against a blunt 27g needle to yield a narrowing 0.4mm in diameter upon removal of the needle.

Sham model

For age-matched normal controls, mice underwent thoracotomy alone.

Echocardiography

Pulmonary artery and aortic pressure gradients were measured by pulse wave doppler to confirm PAB or TAC. For LV assessment, M-mode images were acquired in the parasternal short axis view to obtain: LV end systolic and diastolic diameters (LVESD, LVEDD) and LV fractional shortening (FS). For RV assessment, M-mode images were acquired in the apical 4-chamber view to obtain TAPSE. B-mode images were acquired in the apical 4-chamber view to obtain: diastolic RV dimensions at mid-cavity (RVD,mid), and at the base or tricuspid annulus (RVD,base); and RV fractional area change (RV FAC). The lateral tricuspid annular systolic velocity (RV S') was acquired using Doppler tissue imaging in the apical 4-chamber view.

Hemodynamic assessment of RV function

Surgical plane anesthesia was achieved and maintained using 1-2% inhaled isoflurane via noninvasive nose cone. Mouse body temperature was maintained at 37°C using heating pads. With the animal lying supine, the neck was surgically dissected to expose and isolate the right external jugular vein. A 6-0 silk tie was placed at the distal end of the vein with an overhand loop at the proximal end. Following transverse venotomy of the right external jugular vein, a Millar PVR-1035 (Millar Instruments, Houston, TX) mouse conductance catheter was inserted into the vein and advanced through the superior vena cava and right atrium into the RV. The proximal suture was then tightened around the vessel and catheter. Upon hemodynamic stability, steady state baseline data were collected by the conductance catheter coupled to a Millar MPVS Ultra (Millar Instruments, Houston, TX) and PowerLab 16/35 data acquisition system (AD Instruments, Colorado Springs, CO). RV pressure and volume waveforms were recorded simultaneously and analyzed over a minimum of 10 consecutive cardiac cycles using LabChart 8 software (AD Instruments, Colorado Springs, CO). Conductance catheter was calibrated using the cuvette method and freshly heparinized warm blood and then zeroed in warm saline.

Neonatal rat ventricular myocyte isolation and culture

Neonatal Sprague-Dawley rats were euthanized by decapitation within the first 24h after birth and beating hearts were collected in 1xPBS (Corning-LDP) containing penicillin (100 units/ml) / streptomycin (100 μg/ml) (Gibco-Fisher Scientific). Ventricular tissue was dissected, further minced, rinsed in 1xPBS, and then digested in 0.1% Trypsin in 1xPBS for 15min at 37ºC. Supernatant was collected and the remaining tissue was further digested repeatedly for a total of 10 times, with serial collection of supernatant. Digestion was stopped on ice with 10% FBS. Cells were collected from pooled supernatant by centrifugation (1500 rpm for 5 min at room temperature). The cell pellet was resuspended in complete medium. Cells were counted and plated in 10 cm dishes for ~1h at 37°C, 5% CO_2 at a density of $10x10^6$ cells per plate (pre-plating). During pre-plating, non-myocytes adhere to the plate, while NRVMs remain in suspension. The supernatant cells were subsequently seeded on protamine sulfate coated dishes (10^5 cells/cm^2) and left to attach for 12h. NRVM primary cultures were maintained in MEM medium supplemented with 10% FBS, penicillin (100 units/ml) / streptomycin (100 μg/ml) (Gibco-Fisher Scientific). 1-β-D-Arabinofuranosyl-cytosine (AraC 20 μM, Calbiochem-Sigma) was added to culture medium to inhibit fibroblast proliferation.

MitoSOX Red Analysis

Briefly, cells were incubated with 2.5 μM of MitoSOX™ Red mitochondrial superoxide indicator (Molecular Probes) in serum free culture medium for 20 min at 37ºC protected from light. Cells were washed with warm medium and imaged with a DMI8 fluorescent microscope (Leica) using a red fluorescent filter (excitation/emission 510/580 nm). Cells incubated with H_2O_2 (50 μM) for 2h were used as positive control. Red fluorescent signal was measured with ImageJ software and normalized to brightfield signal.

MTT assay of cell viability

To assess NRVM viability, the Vybrant MTT cell proliferation assay kit was used (Molecular Probes). NRVM were seeded on 96-well plates at ~$3x10^4$ cells/well (~10^5 cells/cm^2) and treated identically as in the siRNA transfection assays (including transfection, serum starvation and neurohormonal stimulation). A standard curve was created to calculate the linearity between absorbance at 595nm and cell number. Prior to labelling with MTT, the medium was removed and 100 µl of fresh medium was added to each well. Medium without cells was used as negative control (blank). The cells and negative control were labeled with 10 µl of 12 mM MTT/well and incubated at 37°C for 4h. Subsequently, SDS-HCL (100 µl) was added to each well, mixed thoroughly, and incubated for 4h at 37°C. Absorbance at 595 nm was measured on a plate reader and the % of cell viability was calculated using the formula:

$$\% \text{ of viability} = (A595_{sample} / A595_{reference}) \times 100$$

Redox Western blots

In NRVMs, the redox state of the mitochondrial proteins CYPD and TRX2 was estimated by redox Western blot as previously described (75). Briefly, NRVMs were transfected with si-*Wipi1* or si-scramble and incubated at 37°C under the following conditions: 1) non-treated control (18h); 2) N-Acetyl cysteine (NAC, 2 mM, 18h); 3) hydrogen peroxide (H_2O_2, 0.1 mM,18h); and 4) aldosterone (Aldo, 1µM, 48h). Cells were harvested in urea lysis buffer (8 M urea, 50 mM Tris/HCl (pH 8.3) and 1 mM EDTA) containing 20 mM IAM and incubated for 30 min at 37°C to alkylate protein thiol groups. Protein was precipitated from lysate supernatant with cold acetone-1M HCl (98:2,v/v), washed with acetone-1 M HCl-H2O (98:2:10, v/v/v), centrifuge pelleted, and then resuspended and incubated for 30min at 37 °C in urea lysis buffer containing 5 mM DTT to reduce the oxidized protein thiol groups. Subsequent incubation in IAA (100 mM) in urea/DTT lysis buffer (final IAA concentration 50mM) for 30 min at 37 °C was performed to alkylate DTT-reduced thiol groups. Alkylation reactions were performed in the dark. After modified BCA assay estimation of protein content, samples were subjected

to urea-PAGE electrophoresis (7 M urea and 7.5% acrylamide) in non-reducing conditions and immunoblotted for CYPD and TRX2.

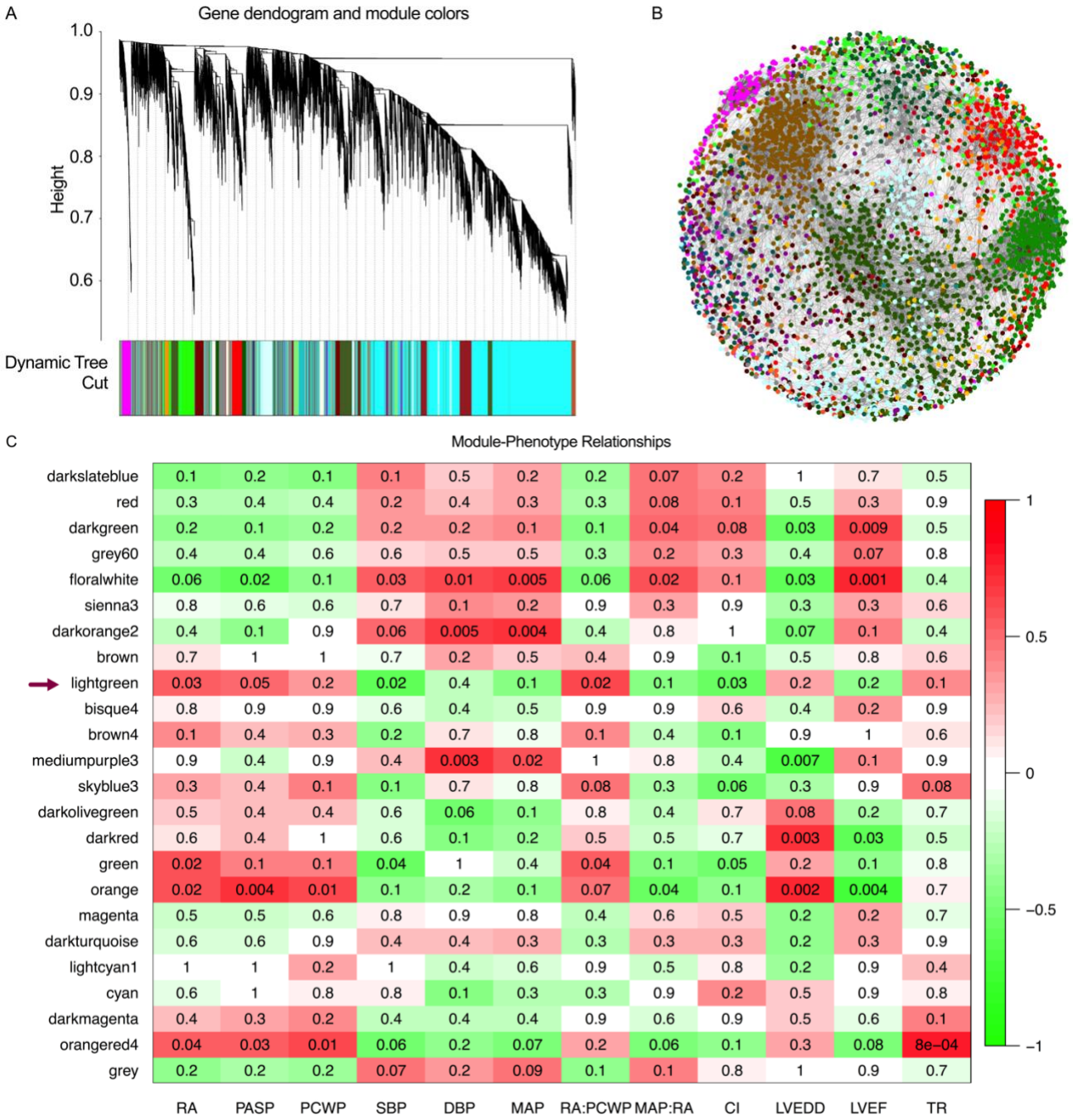

Supplemental Figure S1. Weighted gene co-expression network analysis (WGCNA) gene dendrogram, modules, and module-phenotype correlation analysis. (A) Gene modules were identified using WGCNA dendrograms derived from the right ventricular transcriptome. The dynamic tree-cut algorithm was used to identify break points in the gene-tree, thereby indicating different clusters of related genes. (B) Cytoscape visualization of the 23 RV-derived gene network modules identified. Color represents a distinct module. Line intensity and length indicate strength of individual interactions between gene pairs. Darker, shorter lines represent stronger connections than lighter, longer lines. (C) Module-phenotype relationship heatmap matrix for hemodynamic and echocardiographic indices was created to identify a module associated with right ventricular failure (RVF). Matrix cell color reflects Pearson's correlation value of module-to-phenotype. Correlation *p*-values are shown in cells. The lightgreen module was positively correlated with RA and RA:PCWP and negatively correlated with CI, independent of LVEDD and LVEF, thereby standing out as being associated with RVF. RA, right atrial pressure; PASP, pulmonary artery systolic pressure; PCWP, pulmonary capillary wedge pressure; SBP, systolic BP; DBP, diastolic BP; MAP, mean arterial pressure; CI, cardiac index; LVEDD, left ventricular end-diastolic diameter; LVEF, LV ejection fraction; TR, tricuspid regurgitation.

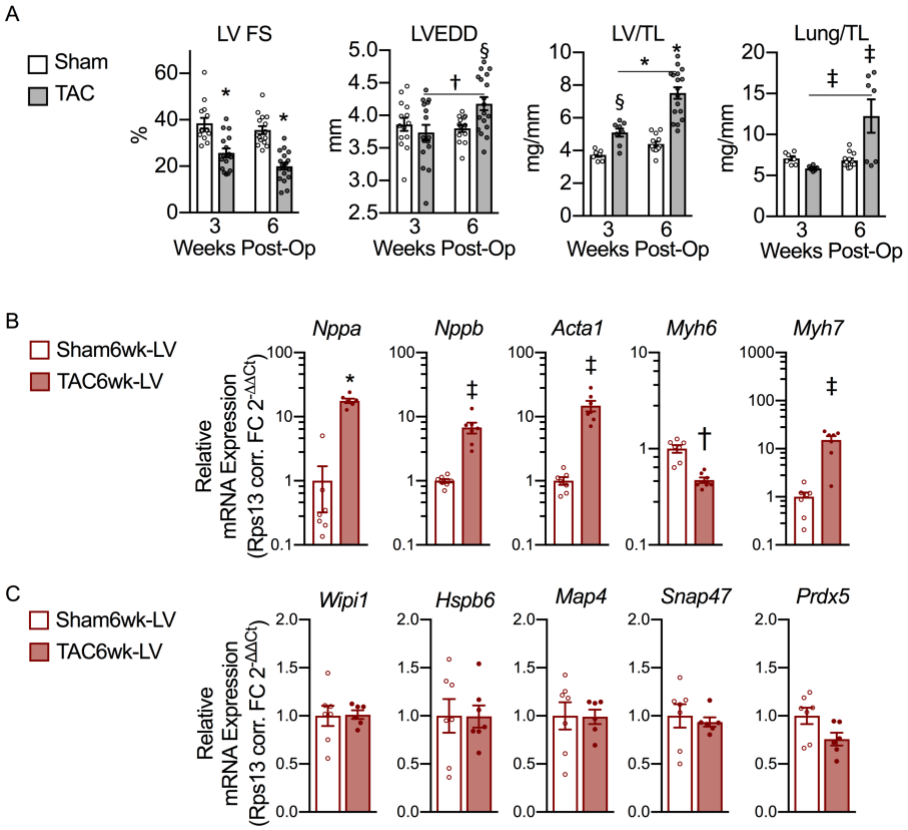

Supplemental Figure S2. Expression of WGCNA-identified RVF-associated gene hub, drivers, and repressor do not change in the failing left ventricle (LV). C57BL/6J WT male mice were subjected to Sham or transverse aortic constriction (TAC) and assessed at 3- and 6-wk post-surgery. **(A)** Serial echocardiograms and terminal morphometrics reveal changes in LV function (LV FS, LV fractional shortening), LV dilatation (LVEDD, LV end-diastolic diameter), LV hypertrophy (LV/TL, LV weight/tibia length ratio), and pulmonary edema (Lung/TL, lung weight/tibia length ratio) over time. n=7-18 per group. RT-qPCR analysis of **(B)** fetal gene program and **(C)** WGCNA-identified RVF-associated gene hub, drivers, and repressor. n=6-8 per group; *p<0.0001, †p<0.01, §p<0.05, ‡ p<0.001 versus respective Sham, unless otherwise indicated by comparison bar, on Tukey's multiple comparison test following two-way ANOVA for panel A, and on two-tailed, unpaired Student's t-test for panels B, C. Scatter dot plots show individual values and mean±SEM.

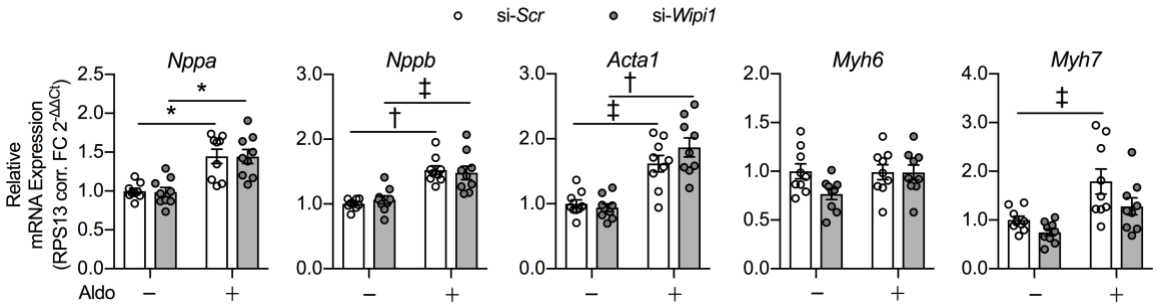

Supplemental Figure S3. Effect of silencing *Wipi1* on aldosterone induction of fetal gene program in neonatal rat ventricular myocytes (NRVMs). NRVMs were transfected with scramble or *Wipi1*-specific siRNAs and stimulated with aldosterone (Aldo, 1μM, 48h). Fetal gene program is induced by Aldo stimulation. Silencing *Wipi1* blunts aldosterone-induced upregulation of *Myh7* (*n*=9 per group from 3 independent experiments). *p<0.001, †p<0.0001, and ‡p<0.01 on Tukey's multiple comparison testing following two-way ANOVA. Scatter plots with bars show individual values and mean±SEM.

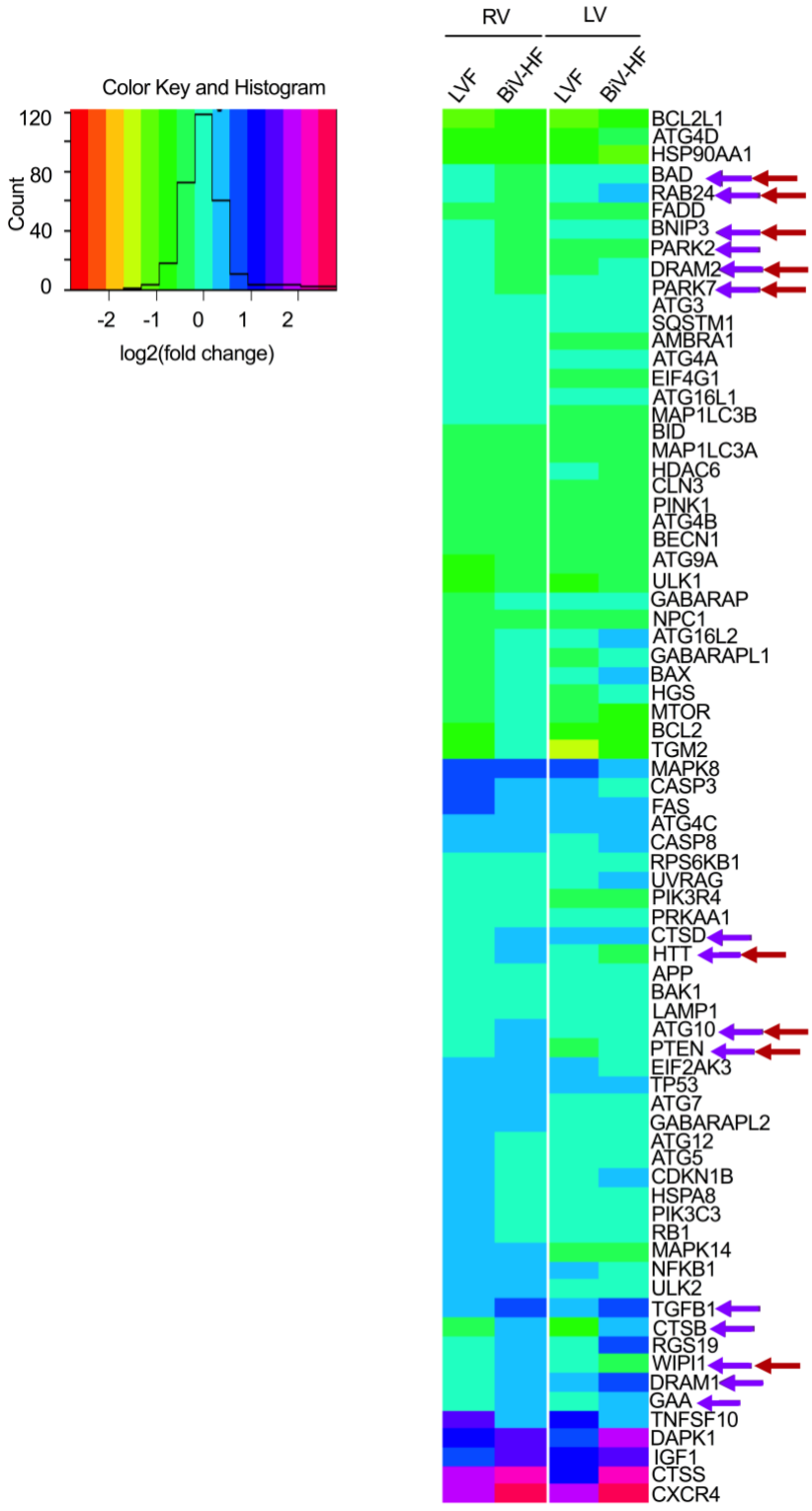

Supplemental Figure S4. Heat map of autophagy genes from human ventricular transcriptomic analysis. Color key shows differential expression (log2(fold change)) relative to respective non-failing ventricle. RV, right ventricle; LV, left ventricle; LVF, LV failure without hemodynamically significant RV failure; BiV-HF, biventricular failure with hemodynamically significant RV failure. Purple arrows, genes that were differentially expressed in the failing RV (BiV-HF RV) and that distinguish the failing RV from the dysfunctional RV (LVF RV). Red arrows, genes that were differentially expressed in the failing RV (BiV-HF RV) and that distinguish the failing RV from the failing LV (BiV-HF LV). *n*=5 per group, per ventricle. Group means are represented in the heat map.

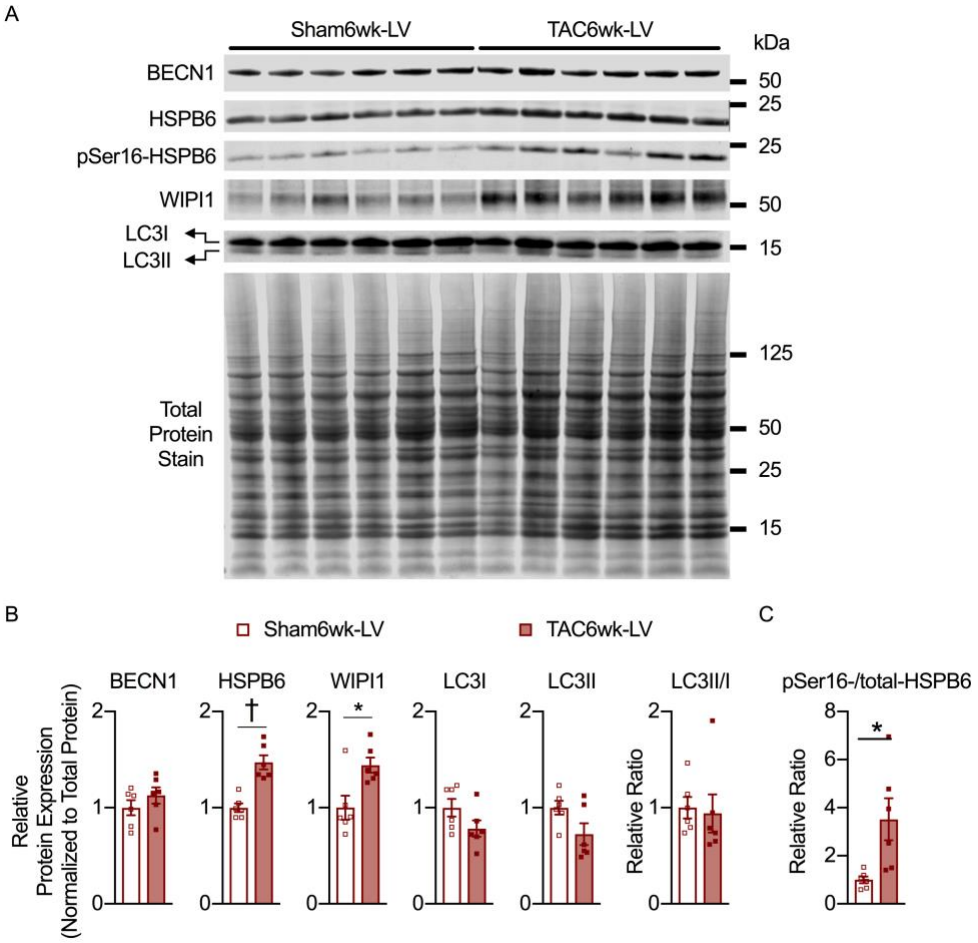

Supplemental Figure S5. Upregulation of canonical autophagy in transverse aortic constriction (TAC)-induced left ventricular failure. Protein lysates were prepared from the left ventricle (LV) of adult C57BL/6J WT male mice subjected to Sham or TAC for 6wk. **(A)** Western blots of autophagy proteins and total protein stain. **(B)** Summary Western analyses. Upregulation of select autophagy proteins in the absence of increased LC3 lipidation in TAC6wk-LV versus Sham6wk-LV suggests that overall autophagic flux is unchanged in the failing versus non-failing LV. **(C)** Increased Ser16-phosphorylation of HSPB6 in TAC6wk-LV suggests a shift towards increased canonical autophagy in the failing LV. *p<0.05, †p<0.001 on two-tailed Student's t-test; *n*=6 per group. Scatter dot plots show individual values and mean±SEM.

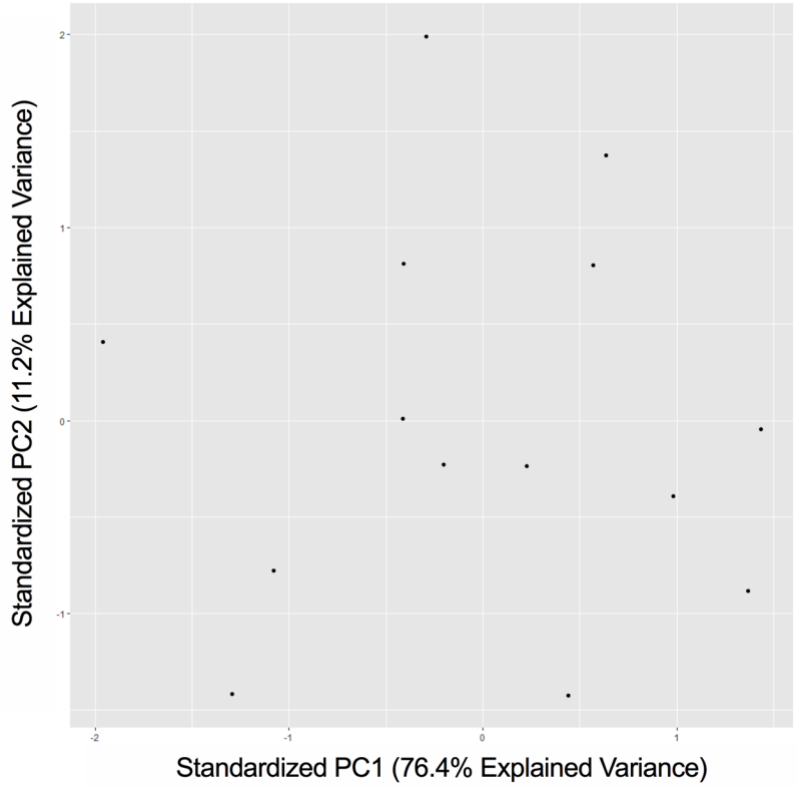

Supplemental Figure S6. Principal component analysis plot of right ventricular failure-associated module. The first principal component accounts for the vast majority (76.4%) of the information in the module.

		NF (n=5)	LVF (n=5)	BiV-HF (n=5)
Demographics	**Age (yrs),** mean ±SEM median (IQR)	49.0±3.4 51.0 (9)	61.6±1.1 62 (1)	61.8± 2.2 60.0 (4)
	Gender (%male)	20	60	100
Co-Morbidities & Past Medical History	**Hypertension (%)**	100	40	40
	Diabetes Mellitus (%)	20	20	20
	Atrial Fibrillation (%)	0	20	40
	CAD (%)	0	100	100
	h/o MI (%)	0	80	80
	h/o CABG (%)	0	100	60
Medications	**ACEi/ARB/MRA (%)**	0	80	80
	β-blocker (%)	80	80	20
	Hydralazine (%)	0	20	0
	Nitrate (%)	0	100	80
	Digoxin (%)	0	60	60
	Diuretic (%)	20	60	60
Circulatory Support	**Inotropic support (%)**	0	40	100
	IABP (%)	0	20	20
Echo Parameters	**LVEF (%)**	57.5±4.5	25.0±3.4	12±2.3
	LVEDD (cm)	4.4±0.3	6.6±0.4	7.0±0.4
	MR Severity (n)			
	None	4	2	0
	Mild	1	2	2
	Moderate	0	1	3
	Severe	0	0	0
	TR Severity (n)			
	None	3	4	1
	Mild	2	1	2
	Moderate	0	0	1
	Severe	0	0	1

Supplemental Table S1. Clinical characteristics of non-failing patients and heart failure patients with and without biventricular failure. NF, non-failing; LVF, left ventricular failure without hemodynamically significant right ventricular failure; BiV-HF, biventricular heart failure; CAD, coronary artery disease; h/o, history of; CABG, coronary artery bypass graft surgery; ACEi, angiotensin converting enzyme inhibitor; ARB, angiotensin receptor blocker; MRA, minerolacorticoid receptor antagonist; β-blocker, beta-adrenergic receptor blocker; IABP, intra-aortic balloon pump.

	NF	LVF	BiV-HF	P value
RA (mmHg)	7.2±1.7	4.0±0.5	25.8±1.7*†	<0.0001
PASP (mmHg)	27.4±2.2	26.0±1.5	67.0±1.8*†	<0.0001
PCWP (mmHg)	14.8±2.2	10.6±1.1	25.6±2.6**‡	<0.001
RA:PCWP	0.46±0.07	0.38±0.03	1.05±0.11***‡	<0.001
MAP:RA	17.2±4.5	22.3±2.9	2.8±0.3**§	<0.01
CI (L/min/m^2)	3.7±0.2	3.3±0.4	2.2±0.2**§	<0.01
SBP (mmHg)	130.6±6.2	121.8±5.4	99.4±6.6**#	<0.01
DBP (mmHg)	79.6±4.5	64.2±7.2	56.8±4.7**	0.04
MAP (mmHg)	96.6±4.8	83.4±5.6	71.0±3.6**	<0.01

Supplemental Table S2. Hemodynamic parameters of BiV-HF and LVF patient cohorts. RA, right atrial pressure; PASP, pulmonary artery systolic pressure; PCWP, pulmonary capillary wedge pressure; MAP, mean arterial pressure; CI, cardiac index; SBP, systolic blood pressure; DBP, diastolic blood pressure. ANOVA p value shown in table. * $p < 0.0001$ vs. NF; ** $p < 0.05$ vs. NF; *** $p<0.001$ vs. NF; † $p < 0.0001$ vs. LVF; ‡ $p < 0.001$ vs. LVF; § $p < 0.05$ vs. LVF; # $p<0.1$ vs. LVF on Tukey's multiple comparison test.

Hub Gene Name	Betweenness Centrality	Significance P-value	FPKM (Mean±SEM)						P values		
			NF_RV	LVF_RV	BiV-HF_RV	NF_LV	LVF_LV	BiV-HF_LV	*RV (BiV-HF vs. NF,LVF)	*LV (BiV-HF, LVF vs. NF)	†BiV-HF RV vs. LV
SBNO2	0.1274	0.00000	10.2±1.4	9.5±2.2	16.4±5.2	11.3±2.8	9.1±1.1	16.7±6.5	0.122	0.769	0.914
TNNI3	0.0854	0.00000	7280.2±790.3	7911.4±860.5	11788.6±2719.9	8702.3±580.7	10755.1±1651.7	11279.0±668.9	0.058	0.094	0.851
ADAP1	0.0558	0.00001	3.8±0.8	5.9±0.8	9.8±2.2	5.1±1.0	6.7±0.8	8.6±1.3	0.014	0.079	0.415
RRBP1	0.0770	0.00002	27.2±2.1	32.5±4.0	39.3±8.5	30.0±6.3	35.2±2.6	38.4±12.5	0.176	0.496	0.854
WIPI1	0.0507	0.00002	32.4±3.2	33.6±1.5	46.2±6.2	40.2±4.0	36.6±3.6	34.8±3.6	0.017	0.329	0.048
ANKRD13D	0.0961	0.00004	7.1±0.6	7.2±1.5	9.3±2.4	6.9±0.6	7.4±1.6	9.0±2.3	0.279	0.521	0.728
ADRA2C	0.0584	0.00004	3.7±0.9	3.6±0.9	6.3±1.6	3.4±0.8	3.0±0.4	6.3±1.3	0.077	0.384	0.947
JBTS26	0.0396	0.00013	3.8±0.3	3.5±0.3	6.2±0.8	5.5±1.0	4.7±0.4	5.3±1.0	0.001	0.634	0.234
DRG2	0.0566	0.00020	12.9±1.0	13.0±0.7	15.1±2.3	13.1±1.1	12.4±1.0	13.5±0.8	0.261	0.910	0.363
XLOC_007409	0.0866	0.00026	1.3+0.6	1.2+0.5	3.9+2.2	0.0±0.0	0.0±0.0	3.3±2.7	0.112	0.419	0.359

Supplemental Table S3. Genetic hubs of RVF-associated module

FPKM, fragments per kilobase of transcript per million mapped read; NF, non-failing; LVF, left ventricular failure without hemodynamically significant RV failure; BiV-HF, biventricular heart failure; RV, right ventricle; LV left ventricle. *Unpaired two-tailed Student's t-test p value, † denotes paired two-tailed Student's t-test p value.

Species	Gene	Primer	Sequence (5'-3')
Mouse Rat	*Wipi1*	Forward	CTTTCAACCAAGACTGCACATC
		Reverse	GTTCATCTGCCGAGGTTTTG
Mouse	*Hsbp6*	Forward	GCTCCTTTACCAGGTTTCTCTG
		Reverse	ATCCAGCAGCACGGAAAAATAC
Rat	*Hsbp6*	Forward	TTTACCGGGTTTTTCCACTCCG
		Reverse	CTTCACATCCAGCAGCACAGA
Mouse	*Map4*	Forward	CCCCAAAGAAACAGAGACAAC
		Reverse	CTGAGAGTGAAACCATGCC
Rat	*Map4*	Forward	CTCCTCTCTGCCCTCTCCC
		Reverse	CCGCCATTCTTTACCACTGC
Mouse	*Snap47*	Forward	GGAGCTGACACAGATCCTGA
		Reverse	CATACGCCGGTTTTGCTTGT
Rat	*Snap47*	Forward	CTTCTGCGCGCTCCTGTTG
		Reverse	AGGCCAGGTGTGAACTCGTA
Mouse	*Prdx5*	Forward	TGGCCTGTCTGAGCGTTAAT
		Reverse	GAGAACCTTTTCAGCCGACG
Rat	*Prdx5*	Forward	ACTATGGCCCCGATCAAG
		Reverse	GGAACAGCCAGGTGTAAATG
Mouse Rat	*Myh6*	Forward	GTGACAGTGGTAAAGGCAAAGG
		Reverse	TCAGATTTTCCCGGTGGAGA
Mouse Rat	*Myh7*	Forward	GCAGCAAGAAGGACCAGACC
		Reverse	TTTCCCAAATCGAGAGGAGTTG
Mouse Rat	*Nppa*	Forward	GCTTCGGGGGTAGGATTGAC
		Reverse	TAGATGAAGGCAGGAAGCCG
Mouse Rat	*Nppb*	Forward	CTTCGGTCTCAAGGCAGCAC
		Reverse	GAGACCCAGGCAGAGTCAGAA
Mouse Rat	*Acta1*	Forward	AGCCTCACTTCCTACCCTCG
		Reverse	TTGTCACACACAAGAGCGGT
Mouse Rat	*Rps13*	Forward	GCACCTTGAGAGGAACAGAA
		Reverse	GAGCACCCGCTTAGTCTTATAG
Mouse	*Rps15*	Forward	TTCTCCATCACCTACAAACCC
		Reverse	ACCAGTCTTTATTGGCCTCG
Rat	*Rps15*	Forward	GTTCTCCATCACCTACAAGCC
		Reverse	ACGAGTCTTTATTGTCCCCAC

Supplemental Table S4. Complete list of primers.

Primary Antibodies	Dilution in WB	Company (Catalog no.)
Anti-WIPI1	1:500	Novus Biologicals (NBP1-88878)
Anti-HSPB6	1:2,000	Fitzgerald (10R-H111A)
Anti-phospho Serine 16 HSPB6	1:1000	Fitzgerald (70R-36849)
Anti-MAP4	1:5,000	Millipore (AB6020)
Anti-SNAP47	1:500	Aviva (ARP58429_P050)
Anti-PRDX5	1:500	Aviva (ARP54832_P050)
Anti-BECN1	1:1,000	Cell signalling (#3738)
Anti-LC3 (I and II)	1:1,000	Bio-Rad (AHP2167)
Anti-CyclophilinD (clone: E11AE12BD4)	1:1,000	Thermo-Fisher (45-590-0)
Anti-Thioredoxin2	1:1,000	Santa Cruz (F-10, sc-133201)
Secondary Antibodies	**Dilution in WB**	**Company (Catalog no.)**
IRDye® 800CW Goat anti-Rabbit IgG	1:10,000	LI-COR Biosciences (926-32211)
IRDye® 680RD Goat anti-Mouse IgG	1:10,000	LI-COR Biosciences (926-68070)
IRDye® 800CW Goat anti-Mouse IgG1 Specific	1:10,000	LI-COR Biosciences (926-32350)
IRDye® 800CW Goat anti-Mouse IgG2b Specific	1:10,000	LI-COR Biosciences (926-32352)

Supplemental Table S5. Complete list of antibodies.